Int J Heat Mass Transfer Vol 33, No 11, pp 2533–2544, 1990
Printed in Great Britain

0017-9310/90 $3 00+0 00

Prandtl number effects on the stability of natural convection between spherical shells

ROD W DOUGLASS,† KEVIN G TEBEEST,† STEVEN A. TROGDON‡ and DAVID R GARDNER§

†Computational Mechanics Laboratory, Department of Mechanical Engineering, 255 Walter Scott Engineering Center, University of Nebraska-Lincoln, Lincoln, NB 68588-0656, U.S A
‡Department of Mathematics and Statistics, University of Minnesota–Duluth, Duluth, MN 55812-2496, U S A
§Theory and Analysis Division, Sandia National Laboratories, Albuquerque, NM 87185, U S A

(*Received* 15 *August* 1989 *and in final form* 17 *January* 1990)

Abstract—An analysis of the effect of the Prandtl number on the linear stability of axisymmetric ($m = 0$) disturbances on steady natural convection contained between two concentric spherical shells when the gap is narrow are presented. The disturbance equations are solved using a truncated spectral series. Convergence of the series is examined. Prandtl numbers range from 0 to 100 while the relative gap-width is either 0 100, 0.075, or 0.050 Results confirm the hypothesis that experimentally observed changes in the basic motion for certain flow parameters are due to its instability and indicate that for any Prandtl number larger than a transition value, the unstable flows evolve to a steady pattern while for smaller Prandtl numbers the bifurcated flows are time periodic

1. INTRODUCTION

PRESENTED in this article are the results of a numerical linear stability analysis of steady natural convection between concentric narrow-gap spherical shells. The boundaries are of uniform, but different temperatures, with the inner surface being the warmer Gravity acts uniformly parallel to the vertical axis which passes through the common centers of the spheres. An Oberbeck–Boussinesq fluid fills the annulus. Model fluids are selected such that Prandtl numbers range from 0 to 100, where the $Pr = 0$ case is an idealization of a viscous fluid in which thermal disturbances are communicated instantaneously throughout the fluid An extensive study of the stability of the basic motion is done for a relative gap-width of $\varepsilon = 0\ 100$ with additional data presented for values of $\varepsilon = 0\ 075$ and $0\ 050$

Properties of the basic motion and other related results are detailed in ref [1] Similar parameter values were used in ref. [1] for the problem considered here, however an error in the basic motion for flows having a warmer inner boundary caused the stability results and conclusions to be incorrect Their general analysis, however, remains correct. We present here, a more thorough convergence analysis of the numerical solutions as well as a more complete exploration of the dependence of the critical stability parameter on the Prandtl number for the correct basic motion

A neutral stability map for convection of air in a wide range of gap-widths is shown in Fig. 1 The map is based on flow visualization data of Bishop *et al* [2] and Yin *et al.* [3, 4] The main point of the illustration is the occurrence of regions of parameter space wherein the flows are observed to be either steady or unsteady. It is the hypothesis of the work reported here that the occurrence of flow transitions is due to the hydrodynamic instability of the basic motion rather than being a result due to errors in the experimental method. The results shown here demonstrate

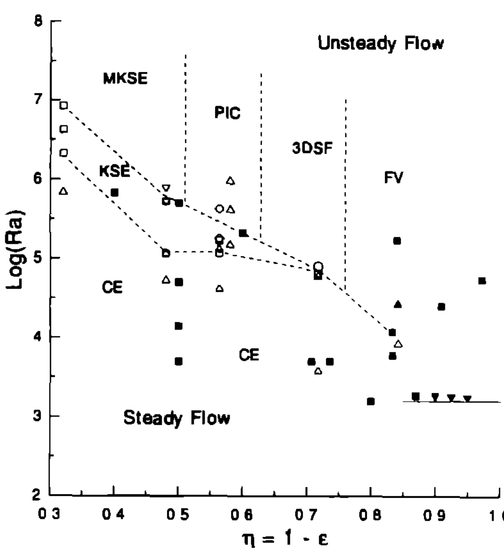

FIG 1 Summary of parameter values used in flow visualization experiments and numerical simulation of the basic motion for air in the spherical annulus Flow visualization data suggest six different types of flow CE, crescent eddy (△), KSE, kidney-shaped eddy (□), MKSE, modified kidney-shaped eddy (▽); PIC, periodic internal contracting eddy (◇), 3DSF, three-dimensional spiral flow (○), FV, falling vortices (▲) [2, 4]. Only the CE and KSE regions have steady flows. Values of ε and *Ra* used in computing the steady basic motion [9–14] (■) which lie above the CE and KSE regions may not represent the true flow field Computed critical Rayleigh numbers $Ra_c = \mathscr{R}_c^2\ Pr$ for a Prandtl number of 0.7 obtained here are indicated by (▼) The solid horizontal line represents the Rayleigh–Bénard limit of $Ra_c = 1708$

NOMENCLATURE

$C(\varepsilon)$ proportionality coefficient
$\mathscr{D}$ problem domain
g gravitational acceleration constant [m s^{-2}]
g_{li}, h_{li} partial spectral expansion functions
Gr Grashof number, $g\beta\Delta T(\Delta r)^3/v^2$
Gr_c critical Grashof number
i $\sqrt{-1}$
m longitudinal wave number
N_c number of terms in Chebyshev (radial) expansion
$\tilde{N}_c$ minimum value of N_c for convergence
N_p number of terms in Legendre (latitudinal) expansion
$\tilde{N}_p$ minimum value of N_p for convergence
N_0 number of zeros of $P_{\tilde{N}_p}$ plus 1
$P_n(x)$ Legendre polynomial of degree n
Pr Prandtl number, v/α
Pr_t transitional Prandtl number
r dimensionless radial coordinate, $(1-\varepsilon)/\varepsilon \leqslant r \leqslant 1/\varepsilon$
r_i, r_o inner and outer radii of the spheres [m]
$\mathscr{R}$ dimensionless stability parameter, $\sqrt{(Gr)}$
$\mathscr{R}_c$ critical value of $\mathscr{R}$
Ra Rayleigh number, $Gr\ Pr$
Ra_c critical Rayleigh number
s stretched eigenvalue, $\sigma\mathscr{R}$
t dimensionless time [s]
$\hat{T}$ disturbance temperature field
$T_n(z)$ Chebyshev polynomial of degree n
T_i, T_o inner and outer surface temperatures [K]
T_0 dimensional base flow temperature field
$\hat{\mathbf{v}}$ disturbed flow velocity vector (v_r, v_τ, v_ϕ)
v_r, v_τ, v_ϕ radial, latitudinal, and longitudinal disturbance velocity components
x transformed latitudinal coordinate, $\cos\theta$
$Y_l^m(x, \phi)$ spherical harmonics
z transformed radial coordinate, $-1 \leqslant z \leqslant 1$
$Z_{\tilde{N}_p}$ number of zeros of $P_{\tilde{N}_p}$

Greek symbols
α thermal diffusivity [m^2 s^{-1}]
β coefficient of volumetric thermal expansion [K^{-1}]
$\Gamma, \Delta, \Xi, \Omega$ functions describing the base flow
ε relative gap-width, $1-r_i/r_o$
ζ stretched radial coordinate, $r-(1-\varepsilon)/\varepsilon$
θ latitudinal spherical coordinate
Θ latitudinal 'scale' of disturbance cells
v kinematic viscosity [m^2 s^{-1}]
ρ fluid density [kg m^{-3}]
σ eigenvalue, $s/\mathscr{R}$
σ_c real part of the critical value of σ
ϕ longitudinal spherical coordinate
$\hat{\Phi}$ disturbance poloidal potential function
ψ base flow stream function
$\hat{\Psi}$ disturbance toroidal potential function

Subscripts
a axisymmetric quantity
c value at criticality
i value at inner radius
o value at outer radius

Superscripts
m longitudinal wave number
$*$ scales for dimensional quantities

that unsteady flows can evolve from situations where steady boundary conditions persist, hence providing evidence confirming that the hypothesis is true

2. THE BASIC AND DISTURBED FLOW

In this section, the basic motion, the linear stability evolution equations, and the solution method are outlined A thorough discussion may be found in ref [5]

2.1 *The basic motion*

The basic motion is the steady natural convective flow of an Oberbeck–Boussinesq fluid induced by a constant temperature difference between the spherical boundaries, the inner surface being the warmer Nondimensionalization of length, temperature, velocity, time, and pressure is accomplished by using the following scales:

$$L^* = \Delta r = r_o - r_i$$
$$T^* = \Delta T = |T_o - T_i|$$
$$V^* = \sqrt{(g\beta\Delta T\Delta r)}$$
$$t^* = L^*/V^*, \quad \text{and}$$
$$P^* = \rho(V^*)^2$$

The solution to the Boussinesq equations of motion was found as a regular perturbation expansion in powers of $\varepsilon = (r_o - r_i)/r_o$, the dimensionless gap-width. The solution is documented in ref. [6] and is found to be

$$\psi(r,x) = (1-x^2)[\Gamma(r,\mathscr{R},Pr,\varepsilon) + x\Delta(r;\mathscr{R},Pr,\varepsilon)] \quad (1)$$

$$T_0(r,x) = T_1(r;\mathcal{R},Pr,\varepsilon)+x[\Xi(r,\mathcal{R},Pr,\varepsilon)+x\Omega(r;\mathcal{R},Pr,\varepsilon)] \quad (2)$$

where $x = \cos\theta$ and the functions Γ, Δ, T_1, Ξ, and Ω are each of the general form

$$\Gamma = \mathcal{R}^m Pr^n \sum_{i=1}^{N} (-1)^i \gamma_i \zeta^i.$$

Forms of these functions specific to this research are given in Appendix I of ref. [5]. The stretched radial coordinate, ζ, is related to the radial coordinate, r, as $\zeta = r-(1-\varepsilon)/\varepsilon$, Pr is the Prandtl number of the fluid, and $\mathcal{R} = [g\beta\Delta T(\Delta r)^3/\nu^2]^{1/2}$ the stability parameter The solution was found to order ε^8, and is valid for [6]

$$\mathcal{R} < \left[\frac{720}{\varepsilon\, Pr}\right]^{1/2}$$

2.2 *The linear stability problem*

The basic motion represented above is to be examined for stability using the usual superposition of an arbitrary disturbance field upon the basic motion and then keeping only those terms with magnitude comparable to the amplitude of the disturbance field. In general, the disturbance field evolves in three dimensions. Here it is assumed a priori that the disturbance flow is two-dimensional, being axisymmetric The axisymmetric analysis leads to upper bounds to the critical stability parameter for the general disturbance field as a function of Prandtl number and dimensionless gap width. The equations governing the general non-linear disturbance field are represented by

$$\mathcal{R}\mathbf{M}\frac{\partial \hat{\mathbf{u}}}{\partial t} = \mathbf{f}_{\hat{u}}(\mathcal{R},\mathbf{U}|\hat{\mathbf{u}})+\mathbf{f}_{\hat{u}\hat{u}}(\mathcal{R},\mathbf{U}|\hat{\mathbf{u}}|\hat{\mathbf{u}}) \quad (3)$$

where $\mathbf{f}_{\hat{u}}$ and $\mathbf{f}_{\hat{u}\hat{u}}$ are respectively linear and bilinear operators The various matrices in equation (3) are defined as

$$\mathbf{U} = \begin{bmatrix} \psi \\ 0 \\ T_0 \end{bmatrix} \quad (4)$$

$$\hat{\mathbf{u}} = \begin{bmatrix} \hat{\mathbf{\Phi}} \\ \hat{\mathbf{\Psi}} \\ \hat{T} \end{bmatrix} \quad (5)$$

$$\mathbf{M} = \begin{bmatrix} \nabla^2\nabla_s^2 & 0 & 0 \\ 0 & \nabla_\tau^2 & 0 \\ 0 & 0 & Pr \end{bmatrix} \quad (6)$$

$$\mathbf{f}_{\hat{u}} = \mathbf{P}\hat{\mathbf{u}} \quad (7)$$

$$\mathbf{f}_{\hat{u}\hat{u}} = \mathbf{N} \quad (8)$$

where $\mathbf{P}$ is a 3×3 linear differential matrix operator and $\mathbf{N}$ a 3-element non-linear vector. $\hat{T}$ is the disturbance temperature field and the quantities $\hat{\mathbf{\Phi}}(r, x, \phi, t)$ and $\hat{\mathbf{\Psi}}(r, x, \phi, t)$ are scalar poloidal and toroidal potential functions, respectively, and are related to the disturbance velocity components, $\hat{\mathbf{v}} = (\hat{v}_r, \hat{v}_\tau, \hat{v}_\phi)$, by

$$\hat{\mathbf{v}} = \hat{\mathbf{v}}_1 + \hat{\mathbf{v}}_2$$
$$\hat{\mathbf{v}}_1 = \mathrm{curl}^2\,(\bar{r}\hat{\mathbf{\Phi}})$$
$$\hat{\mathbf{v}}_2 = \mathrm{curl}\,(\bar{r}\hat{\mathbf{\Psi}})$$

so that the individual components of velocity are then

$$\hat{v}_r = -\frac{1}{r}\nabla_s^2\hat{\mathbf{\Phi}}$$

$$\hat{v}_\tau = -\frac{\sqrt{(1-x^2)}}{r}\frac{\partial}{\partial r}\left(r\frac{\partial\hat{\mathbf{\Phi}}}{\partial x}\right)+\frac{1}{\sqrt{(1-x^2)}}\frac{\partial\hat{\mathbf{\Psi}}}{\partial\phi}$$

$$\hat{v}_\phi = \sqrt{(1-x^2)}\frac{\partial\hat{\mathbf{\Psi}}}{\partial x}+\frac{1}{r\sqrt{(1-x^2)}}\frac{\partial}{\partial r}\left(r\frac{\partial\hat{\mathbf{\Phi}}}{\partial\phi}\right)$$

In these equations

$$\nabla_s^2 f = \frac{\partial}{\partial x}\left[(1-x^2)\frac{\partial f}{\partial x}\right]+\frac{1}{(1-x^2)}\frac{\partial^2 f}{\partial\phi^2}$$

and ∇^2 is the (dimensionless) Laplacian operator in spherical coordinates.

When the disturbance field is axisymmetric, being independent of the longitudinal angle ϕ, the toroidal potential is identically zero (i.e. $\hat{\mathbf{\Psi}} \equiv 0$) The disturbance field can then be represented using the Stokes stream function, where the poloidal potential is related to the stream function $\hat{\Lambda}$ by

$$\hat{\Lambda} = r(1-x^2)\frac{\partial\hat{\mathbf{\Phi}}}{\partial x}.$$

If it is now assumed that the disturbance field is axisymmetric and that the non-linear terms in equation (3) are sub-dominant to the linear terms, the governing system is now

$$\mathcal{R}\mathbf{M}_a\frac{\partial\hat{\mathbf{u}}_a}{\partial t} = \mathbf{f}_{\hat{u}_a}(\mathcal{R},\mathbf{U}_a|\hat{\mathbf{u}}_a), \quad (r,x)\in\mathcal{D} \quad (9)$$

The domain $\mathcal{D}$ is defined as

$$\mathcal{D} = \left\{(r,x)\left|\frac{(1-\varepsilon)}{\varepsilon} < r < \frac{1}{\varepsilon},\quad -1 < x < 1\right.\right\}.$$

The matrix $\mathbf{M}_a$ is the axisymmetric form of the operator $\mathbf{M}$ and $\mathbf{f}_{\hat{u}_a} = \mathbf{P}_a\hat{\mathbf{u}}_a$ Note now that

$$\mathbf{U}_a = \begin{bmatrix} \psi \\ T_0 \end{bmatrix} \quad (10)$$

$$\hat{\mathbf{u}}_a = \begin{bmatrix} \hat{\mathbf{\Phi}} \\ \hat{T} \end{bmatrix} \quad (11)$$

$$\mathbf{P}_a = [\mathcal{P}_{i,j}], \quad i = 1,2, \quad j = 1,2 \quad (12)$$

where

$$\mathscr{P}_{11}(\cdot) = \nabla_a^4\nabla_{s_a}^2(\cdot) - \frac{\mathscr{R}}{r^2}\nabla_{s_a}^2\left[\frac{\partial\psi}{\partial r}\frac{\partial}{\partial x}\nabla_a^2(\cdot)\right.$$

$$\left. + E^2(\psi)\frac{\partial}{\partial x}\mathscr{K}(\cdot)\right] + \frac{\mathscr{R}}{r}\frac{\partial}{\partial r}\left[\frac{1}{r}\frac{\partial\psi}{\partial x}\nabla_a^2\nabla_{s_a}^2(\cdot)\right.$$

$$\left. + \frac{(1-x^2)}{r}\frac{\partial^2\psi}{\partial x^2}\frac{\partial}{\partial x}\nabla_a^2(\cdot)\right]$$

$$+ \frac{\mathscr{R}}{r}\frac{\partial}{\partial r}\left[\frac{1}{r}\frac{\partial}{\partial x}(E^2(\psi)\nabla_{s_a}^2(\cdot))\right]$$

$$\mathscr{P}_{12}(\cdot) = -\frac{\mathscr{R}}{r}\nabla_{s_a}^2((\cdot)x) + \mathscr{R}\mathscr{K}\left[\frac{\partial}{\partial x}((1-x^2)(\cdot))\right]$$

$$\mathscr{P}_{21}(\cdot) = \frac{\mathscr{R}\,Pr}{r}\left[\frac{\partial T_0}{\partial r}\nabla_{s_a}^2(\cdot) - (1-x^2)\frac{\partial T_0}{\partial x}\frac{\partial}{\partial x}[\mathscr{K}(\cdot)]\right]$$

$$\mathscr{P}_{22}(\cdot) = \nabla_a^2(\cdot) + \frac{\mathscr{R}\,Pr}{r^2}\mathscr{J}\left(\frac{(\cdot),\psi}{r,x}\right)$$

The various operators defined in the above system are

$$\nabla_a^2(f) = \frac{1}{r^2}\frac{\partial}{\partial r}\left(r^2\frac{\partial f}{\partial r}\right) + \frac{1}{r^2}\nabla_{s_a}^2(f)$$

$$\nabla_{s_a}^2(f) = \frac{\partial}{\partial x}\left[(1-x^2)\frac{\partial f}{\partial x}\right]$$

$$\mathscr{K}(f) = \frac{1}{r}\frac{\partial}{\partial r}(rf)$$

$$E^2(f) = \frac{\partial^2 f}{\partial r^2} + \frac{(1-x^2)}{r^2}\frac{\partial^2 f}{\partial x^2}, \quad \text{and}$$

$$\mathscr{J}\left(\frac{f,g}{r,x}\right) = \frac{\partial f}{\partial r}\frac{\partial g}{\partial x} - \frac{\partial f}{\partial x}\frac{\partial g}{\partial r}$$

The boundary conditions on $\hat{\mathbf{\Phi}}$ and $\hat{T}$ are

$$\hat{\mathbf{\Phi}} = \frac{\partial\hat{\mathbf{\Phi}}}{\partial r} = \hat{T} = 0 \quad \text{on} \quad \partial\mathscr{D} \qquad (13)$$

where

$$\partial\mathscr{D} = \partial\mathscr{D}_1 \cup \partial\mathscr{D}_2$$

$$\partial\mathscr{D}_1 = \left\{(r,x)|r = \frac{(1-\varepsilon)}{\varepsilon},\ -1 \leqslant x \leqslant 1\right\}$$

$$\partial\mathscr{D}_2 = \left\{(r,x)|r = \frac{1}{\varepsilon},\ -1 \leqslant x \leqslant 1\right\}$$

The initial conditions are arbitrary, but are assumed to be of 'small' amplitude compared to the basic motion and can be represented as a series of a complete set of functions.

2 3 *Solution of the linear system*

The linear system of equations, (9), is solved using the method of normal modes. Let $A(r, x, \phi, t)$ represent an arbitrary disturbance amplitude Then assume that A can be expanded as

$$A(r,x,\phi,t) = \sum_{l=0}^{\infty}\sum_{m=-l}^{l} Y_l^m(x,\phi)A_l^m(r,t) \qquad (14)$$

where the functions $Y_l^m(x,\phi)$ are complete and are called spherical harmonics The index m denotes the wave number in the longitudinal direction, ϕ For axisymmetric disturbances, $m = 0$ so that

$$Y_l^0(x,\phi) = \sqrt{\left(\frac{2l+1}{4\pi}\right)}P_l^0(x)$$

and is independent of ϕ $P_l^0(x)$ is the associated Legendre function of order l and degree 0, which is equivalent to the lth order Legendre polynomial of the first kind These functions are also orthogonal with weight 1 over $-1 \leqslant x \leqslant 1$. Consequently, the solution is composed of functions from a complete set and which are orthogonal, i e a sequence of normal modes. Specifically, let

$$\hat{\mathbf{\Phi}}(r,x,t) \approx \sum_{l=1}^{N_p} g_l(r)P_l(x)\,e^{\sigma_l t} \qquad (15)$$

$$\hat{T}(r,x,t) \approx \sum_{l=0}^{N_p-1} h_l(r)P_l(x)\,e^{\sigma_l t} \qquad (16)$$

where the infinite sum has been truncated to a total of N_p terms and two unknown sets of functions remain: $g_l(r)$ and $h_l(r)$. A finite set of ordinary differential equations for the g_l and h_l functions is obtained after substituting the series (15) and (16) into equation (9) and then applying the orthogonality property of the Legendre polynomials This set of ordinary differential equations is transformed into a series of algebraic equations after applying the Chebyshev-tau method described in ref [7] This solution method requires the radial coordinate to be mapped onto a domain of $[-1, 1]$ using

$$r = \frac{1}{2}\left[z + \frac{2-\varepsilon}{\varepsilon}\right]$$

and that the g and h functions be expanded in a truncated series of Chebyshev polynomials of the form [7]

$$g_l(z) \approx \sum_{i=0}^{N_c} g_{li}T_i(z) \qquad (17)$$

$$h_l(z) \approx \sum_{j=0}^{N_c} h_{lj}T_j(z) \qquad (18)$$

The result of this process is an eigenvalue problem of the form

$$[(\mathbf{B}^{-1}\mathbf{A}) - s\mathbf{I}]\mathbf{x} = 0 \qquad (19)$$

where the eigenvalue $s = \sigma\mathscr{R}$. The matrices $\mathbf{A}$ and $\mathbf{B}$ have elements which depend on the physical parameters of the problem ε, $\mathscr{R}$, and Pr and implicitly on N_p and N_c (until enough terms in the series are included for convergence) The eigenvalues in equation (19) were computed using the EISPACK driver

RG and matrix inversions were carried out using the LINPACK routines SGEFA and SGESL.

For instability, it is required that the eigenvalue with the largest real part in the spectrum of eigenvalues σ found from equation (19) has its real part identical to zero. The imaginary part of that eigenvalue may or may not be zero. If the imaginary part is zero, a *Principle of Exchange of Stabilities* is said to exist. We then wish to search for the set of parameters for which

$$\max\,(\mathrm{Re}\,\{s_i\}) \equiv s_c(\mathscr{R}, Pr, \varepsilon, N_c, N_p) = 0$$

producing a surface of neutral stability of the form

$$\mathscr{R}_c = \mathscr{R}_c(\varepsilon, Pr, N_p, N_c). \qquad (20)$$

The solution procedure used to find equation (20) is summarized in the following algorithm.

(1) *Select a value of* ε *fixing the geometry* ($0 < \varepsilon \leqslant 0.1$)

(2) *Select a value of the Prandtl number, Pr, fixing the fluid to be used.*

(3) *Select a value of* $\mathscr{R}$, *e.g.* $\mathscr{R}_1$.

(4) *Compute the elements of* **A** *and* **B** *in equation* (19)

(5) *Compute the vector of eigenvalues, s, and find the one having the largest real part. Denote this eigenvalue as* s_1

(6) *Check* Re $\{s_1\}$ *if* Re $\{s_1\}$ *is numerically zero, then go to Step* 7. *If* Re $\{s_1\}$ *is greater than zero, then decrement* $\mathscr{R}$ *and repeat Steps* 4 *and* 5. *If* Re $\{s_1\}$ *is less than zero, then increment* $\mathscr{R}$ *and repeat Steps* 4 *and* 5. *Interpolation may be used to find new values of* $\mathscr{R}$

(7) *Compute the critical eigenvector* $\mathbf{x}_c$ *(and the tau coefficients* [7] *if desired).*

(8) *Repeat Steps* 3–7 *for various combinations of* ε *and Pr*

2.4 *Convergence of the approximate solutions*

Of major concern in the solution process is whether or not the truncated series used for the disturbance flow variables has converged. N_p controls the number of terms used in the latitudinal variation of the disturbances through the Legendre polynomials and N_c the number of terms in their radial dependence using Chebyshev polynomials. Let the minimum values for convergence of the Legendre and Chebyshev series be denoted $\tilde{N}_p$ and $\tilde{N}_c$, respectively. Note that in cases for which $Pr \leqslant 100$, $\mathscr{R}$ was computed to three digit accuracy except for $Pr = 0$ and 0.01 where the accuracy was four digits. The effect of N_p and N_c on $\mathscr{R}$ is shown in the following series of figures.

The series of illustrations, Figs. 2–4, show convergence of the spectral series for $Pr = 1$, 10, and 100 for $\varepsilon = 0.100$. This is the widest gap studied. In each case, $\tilde{N}_c = 8$ was sufficient for convergence of the Chebyshev series. There is a slight tendency for $\tilde{N}_p$ to decrease with increasing Pr, being 42 for $Pr = 1$ and 40 for $Pr = 100$. This effect is summarized more completely in Table 1. The apparent sudden decrease in $\mathscr{R}_c$ in Figs. 3 and 4 when N_p changes from 40 to 42 for $N_c = 6$ is a result of the three digit accuracy of the results.

Figures 5–7 show that as the radius ratio increases to $\varepsilon = 0.075$, the value of $\tilde{N}_c = 8$ is sufficient for convergence for all $Pr > 1$. However, substantially more

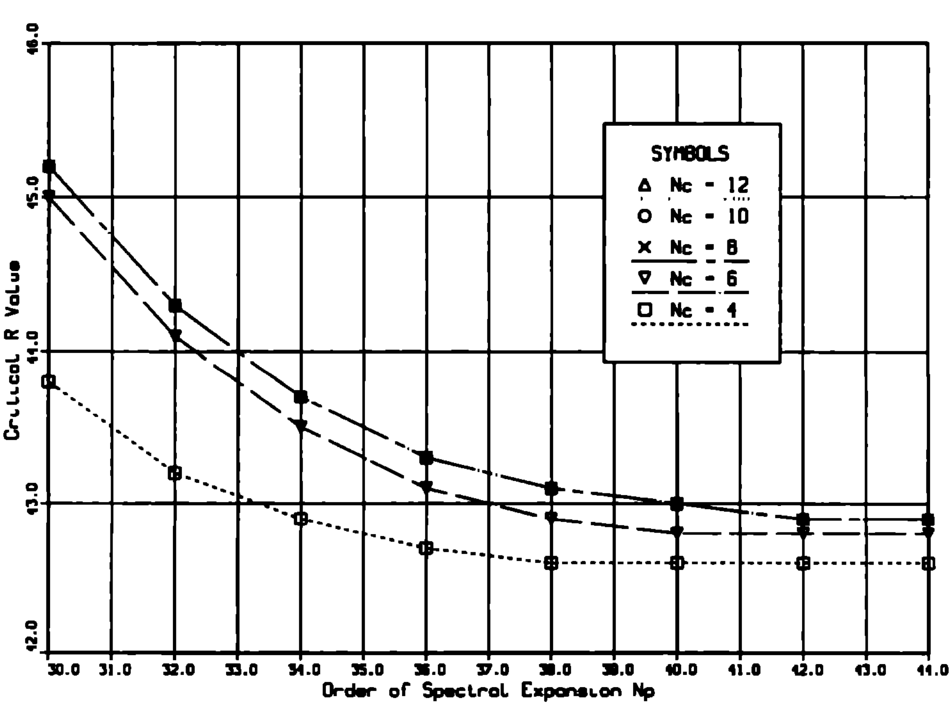

FIG. 2. Convergence study of N_p and N_c for $Pr = 1$ and $\varepsilon = 0.100$

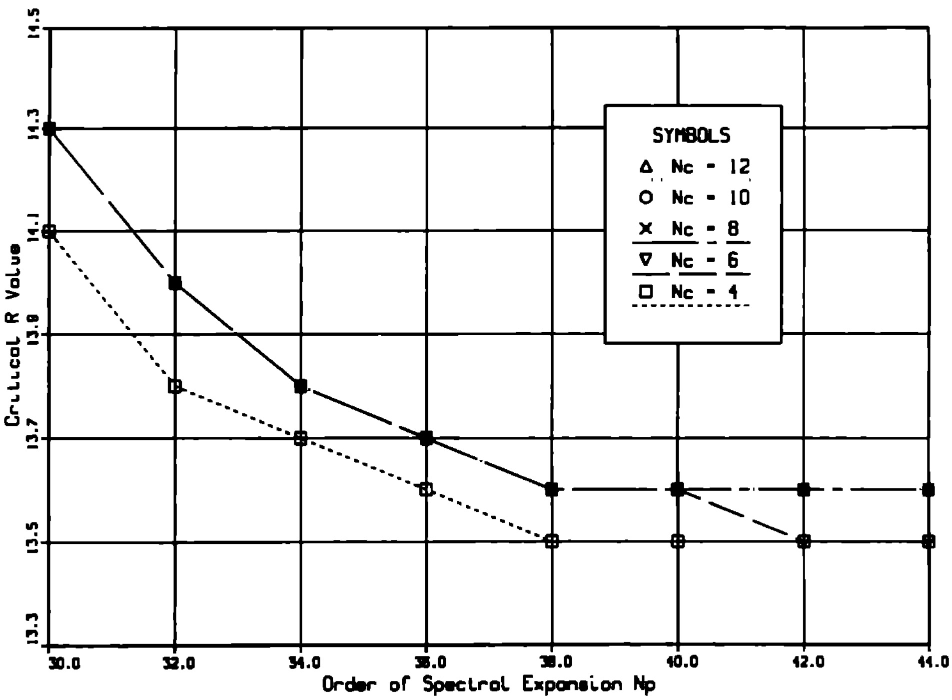

FIG 3 Convergence study of N_p and N_c for $Pr = 10$ and $\varepsilon = 0$ 100

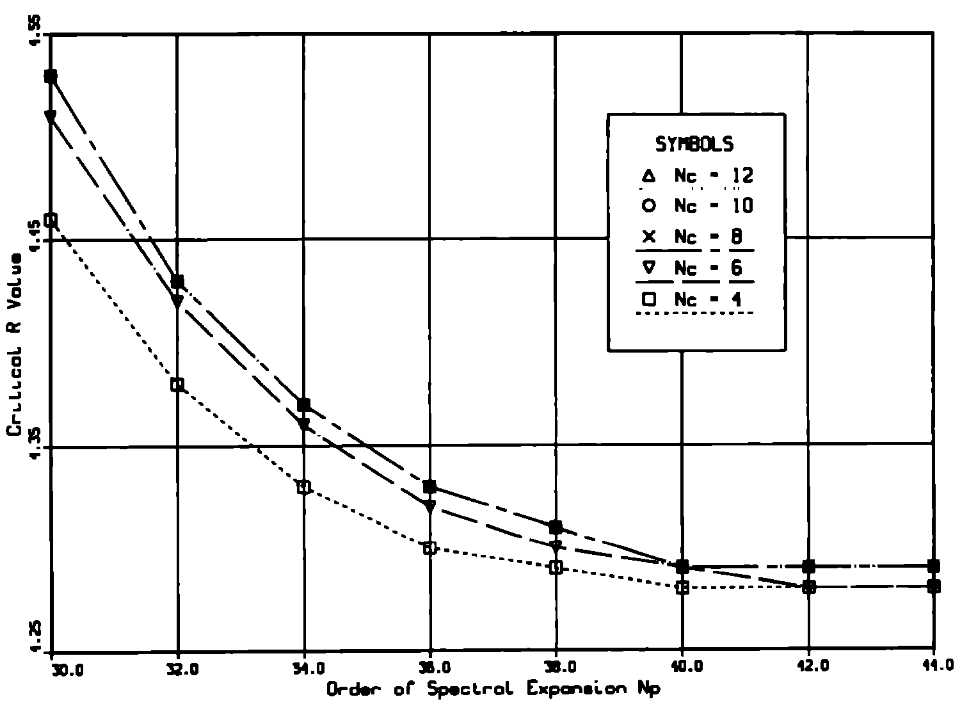

FIG 4 Convergence study of N_p and N_c for $Pr = 100$ and $\varepsilon = 0$ 100

Table 1 Minimum values of N_c and N_p for convergence of $\mathscr{R}_c$ Θ is listed in deg

	Prandtl number, *Pr*											
	<0 3			1			10			100		
ε	$\tilde{N}_c$	$\tilde{N}_p$	Θ	$\tilde{N}_c$	$\tilde{N}_p$	Θ	$\tilde{N}_c$	$\tilde{N}_p$	Θ	$\tilde{N}_c$	$\tilde{N}_p$	Θ
0.100	14	46	3 83	8	42	4 19	8	38	4 62	8	40	4 39
0 075	14	50	3 53	8	52	3 40	4	50	3 53	8	52	3 40
0 050	—	$\gg$70	<2 54	8	~74	<2 40	8	~72	<2 47	8	~74	<2 40

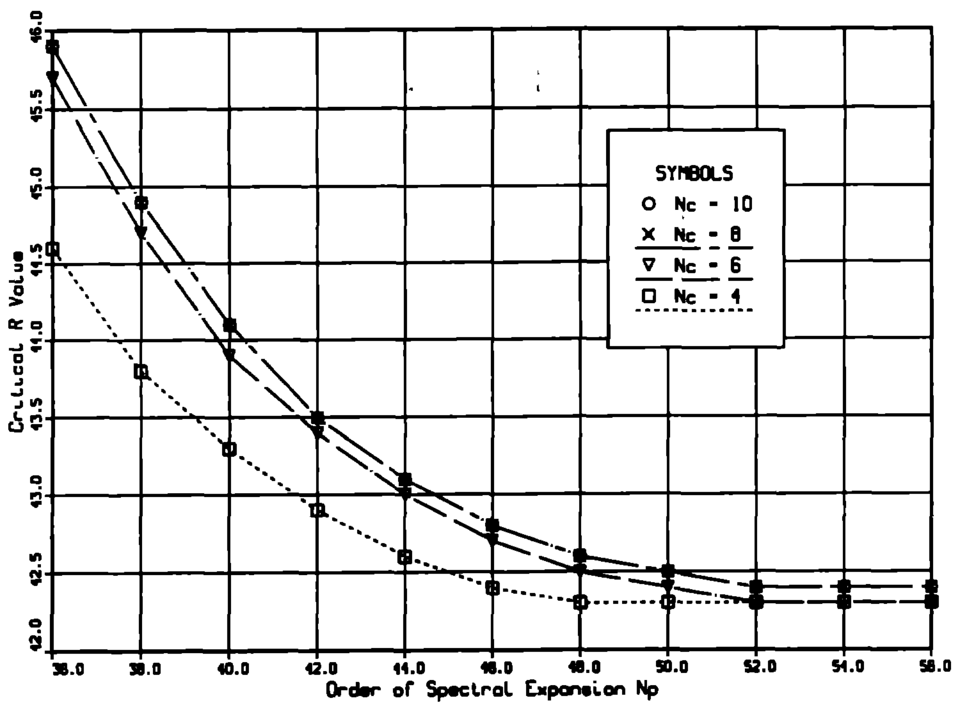

FIG 5 Convergence study of N_p and N_c for $Pr = 1$ and $\varepsilon = 0.075$

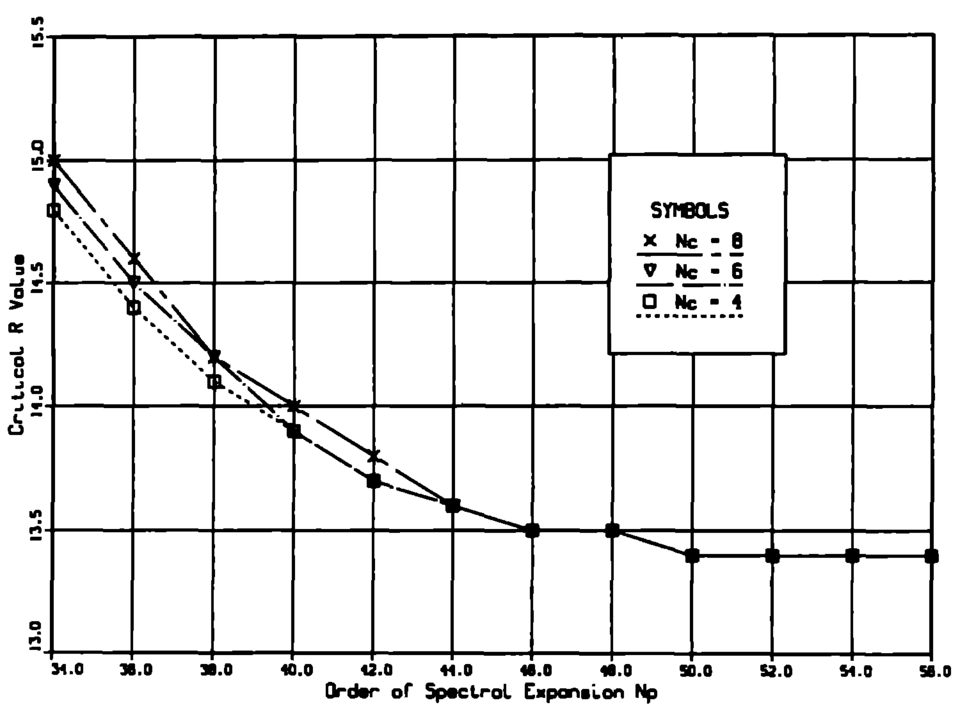

FIG 6 Convergence study of N_p and N_c for $Pr = 10$ and $\varepsilon = 0.075$.

terms are required in the Legendre series, increasing to at least $\tilde{N}_p \approx 50$ This is a reflection of the scale of the disturbance flow in the latitudinal direction As the gap-width decreases, the results indicate that the cells which form the disturbed flow field decrease in latitudinal extent. In order to resolve these smaller scale objects, more terms in the angular dependence approximation are required. An estimate of the size of the small scale structure, Θ, is

$$\Theta \sim \frac{\pi}{N_0} \tag{21}$$

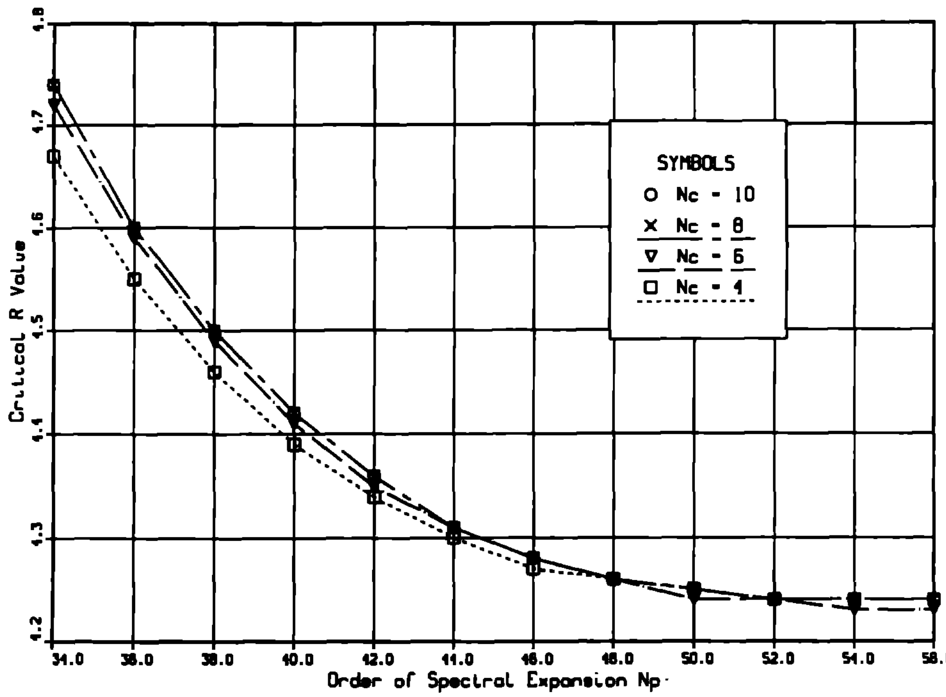

FIG. 7. Convergence study of N_p and N_c for $Pr = 100$ and $\varepsilon = 0.075$.

where

$$N_0 = 1 + Z_{\tilde{N}_p}$$

and where $Z_{\tilde{N}_p}$ is the number of zeros in the Legendre polynomial $P_{\tilde{N}_p}$. For example, for $\varepsilon = 0.075$, $\tilde{N}_p = 52$ and $N_0 = 53$. Then $\Theta \sim 0.0593$ rad (or 3.4°). Results for Θ are summarized in Table 1.

Convergence of the series for $\varepsilon < 0.075$ was similar to the results for $\varepsilon = 0.100$ and 0.075. As indicated in Table 1 values of $\tilde{N}_p$ increase to more than 70! $\tilde{N}_c$ appears to be insensitive to ε, at least for $Pr > 1$.

Inherent in this study is the requirement of large amounts of computing memory. For cases in which $N_p = 70$ and $N_c = 12$, roughly 28 megawords of CRAY 2 main memory was required to perform the computations. From the trends shown in the data, as the gap-width decreases (i.e. $\varepsilon \to 0$), $\tilde{N}_p$ will grow even larger. As Pr decreases toward zero, $\tilde{N}_c$ likewise increases. These trends result in a demand for greater computer memory.

3. THE NEUTRAL STABILITY CURVE

The curve represented by equation (20) when N_p and N_c are fixed at $\tilde{N}_p$ and $\tilde{N}_c$, respectively, has been computed for $\varepsilon = 0.100$ and 0.075. The Prandtl number was varied from 0 to 100. The results are summarized in Fig. 8 and in Table 2. In this figure, $Pr = 0$ is plotted as $Pr = 10^{-4}$.

Recall that the values computed and shown here presume an axisymmetric disturbance field. They will

Table 2. $\mathscr{R}_c$ for axisymmetric disturbances in narrow-gap spherical annuli

	Relative gap-width, ε		
Pr	0.100	0.075	0.050
0.00	108.8	102.2	
0.05	99.6		
0.10	94.2	91.4	
0.21	88.2	87.0	
0.23	87.5	86.3	
0.25	87.0	85.7	
0.27	86.7	85.2	
0.28		85.1	
0.29	86.6	83.2	
0.30	86.3	81.0	
0.305	85.0		
0.31	83.8	79.1	
0.33	79.5		
0.40	69.6	67.7	
0.50	61.3	60.2	
0.70	51.4	50.7	50.3
1.00	42.9	42.4	42.1
2.00	30.3	30.0	
3.00		24.5	
4.00		21.2	
5.00	19.2	19.0	
10.00	13.6	13.4	
20.00	9.59	9.49	
30.00	7.83	7.75	
40.00	6.78	6.71	
50.00	6.07	6.10	
60.00	5.54	5.48	
70.00	5.13	5.07	
80.00	4.80	4.74	4.71
90.00	4.47	4.47	4.44
100.00	4.29	4.24	4.21

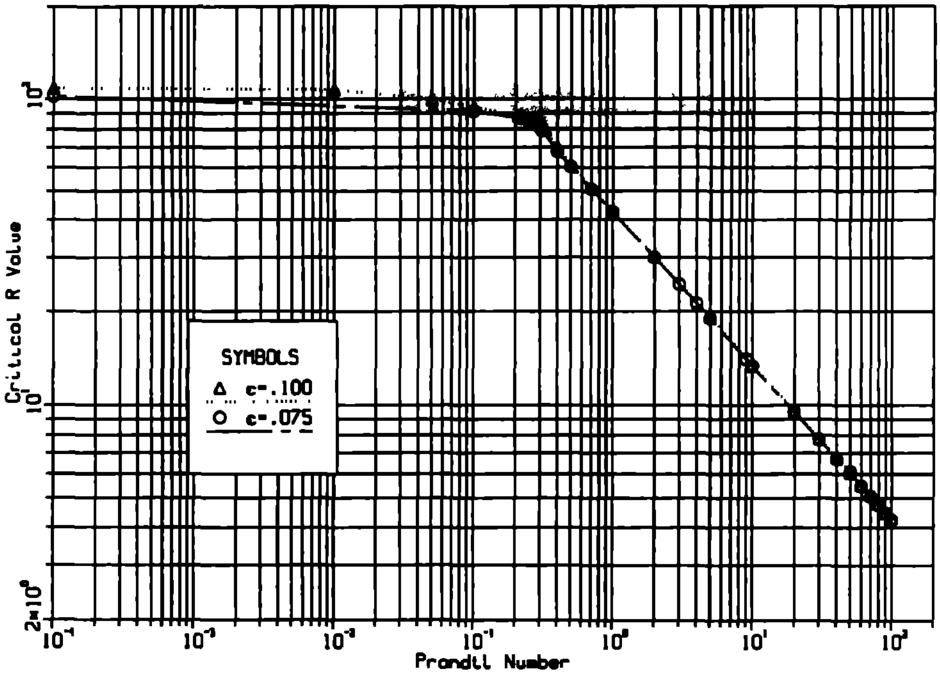

FIG 8 Neutral stability of natural convection between narrow-gap spherical shells

therefore be either the critical values for the problem or their upper bound For, if in equation (14) $m > 0$ and a corresponding value of $\mathscr{R}_{c_{m>0}}$ is found which exceeds that computed for $m = 0$, the basic motion would have already become unstable for the smaller value of $\mathscr{R}_{c_{m=0}}$ As an illustration, Gardner (p. 127 of ref. [5]) found for $Pr = 0.7$ and $\varepsilon = 0$ 1 that the critical wave number was $m = 2$ giving $\mathscr{R}_c = 51.296$. In Table 2, $\mathscr{R}_c = 51$ 4 at $m = 0$ for the same Pr and ε

There are five general comments to be made regarding the neutral curve of Fig 8

(1) The neutral stability curves have upper bounds for each ε, being

$$\mathscr{R}_0(\varepsilon) = \lim_{Pr \to 0} \mathscr{R}_c(\varepsilon, Pr)$$

and are asymptotic to the lines defined by $\mathscr{R}_c(\varepsilon, Pr) = \mathscr{R}_0(\varepsilon)$

(2) The neutral curve is a monotone decreasing function of Pr for each ε

(3) A *transition region* exists over which the neutral curve changes from one structure to another A *transition Prandtl number*, Pr_t, is defined as that value of the Prandtl number which segregates the structures of the neutral curve.

(4) For $Pr > Pr_t$ the neutral curve is linear on a log–log plot

(5) As the dimensionless gap-width decreases, the values of $\mathscr{R}_c$ decrease while keeping the Prandtl number fixed This is more clearly seen in Table 2

The neutral stability curve is asymptotic from below to the line $\mathscr{R}_c = \mathscr{R}_0(\varepsilon)$ and the asymptote, as a function of ε, increases with ε. The specific dependence of the asymptotes on the relative gap-width, ε, is shown in Table 2 as the entries for $Pr = 0$.

The most striking feature of Fig. 8 is the transition from a linear structure to a non-linear structure at the transition Prandtl number, Pr_t In the linear segment, the slope of the line is $-1/2$ on a log–log plot. This indicates that for $Pr > Pr_t$ the critical stability parameter can be correlated as

$$\mathscr{R}_c = \frac{C(\varepsilon)}{\sqrt{(Pr)}}, \quad \text{for} \quad Pr > Pr_t \qquad (22)$$

or that a critical Rayleigh number can be defined over the same Prandtl number range such that

$$Ra_c \equiv Gr_c\, Pr = C^2(\varepsilon)$$

which is independent of Pr The proportionality coefficient $C(\varepsilon)$ is given in Table 3 for $\varepsilon = 0$ 100, 0.075, and 0 050

The transition regions are magnified in Fig. 9 This figure illustrates the linear to non-linear transition in the neutral curve and identifies the values of Pr_t Values of Pr_t are given in Table 3 Gardner (Section 6 3 1 of ref [5]) has shown that the Prandtl number

Table 3 Transition Prandtl numbers and proportionality coefficients, $C(\varepsilon)$, for $Pr > Pr_t$ in equation (22)

Relative gap-width, ε	$C(\varepsilon)$	Pr_t
0 100	42 9	0.30
0.075	42 4	0 28
0.050	42 1	—

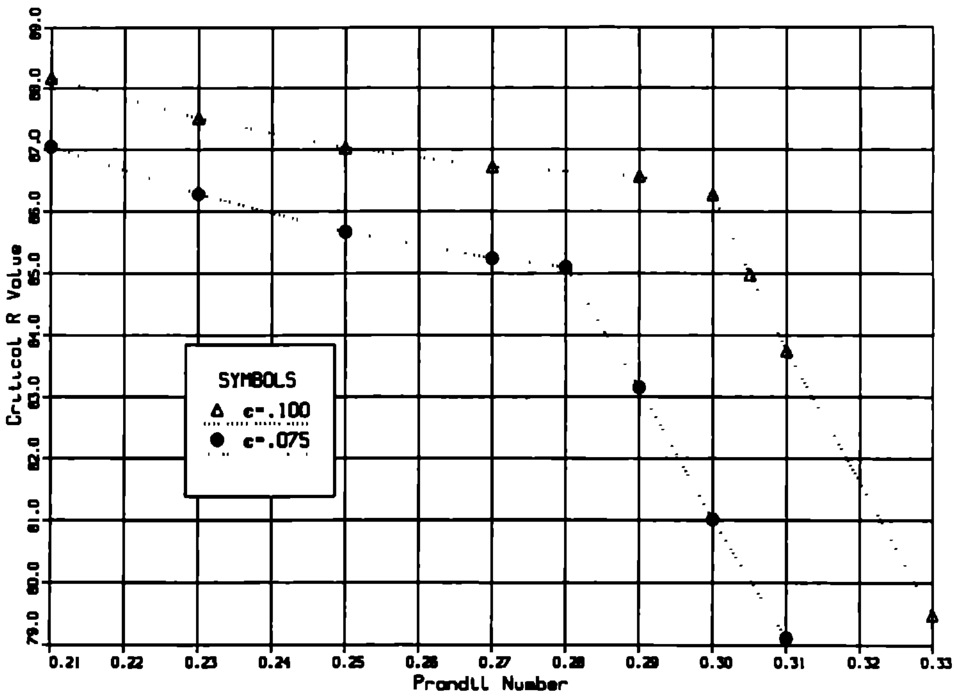

FIG 9 Magnification of the neutral stability curve near the transition Prandtl number showing the change from linear dependence on *Pr* to a non-linear dependence as *Pr* decreases

plays a most important role in the bifurcation of the unstable solutions. As the Prandtl number approaches the transition Prandtl number from above, the imaginary part of the critical eigenvalue changes from zero (i.e. states where a *Principle of Exchange of Stabilities* exists) to a non-zero value below Pr_t. This is not, in fact, an abrupt change in $|\mathrm{Im}\{s_c\}|$, but in the identity of that eigenvalue having the largest real part in the spectrum of eigenvalues. The implication is that for Prandtl numbers greater than Pr_t, the bifurcated flow is steady while it is periodic for smaller values of *Pr*

Table 4 contains the critical eigenvalues for the values of ε and *Pr* in Fig. 9 illustrating the change in the imaginary part of *s* The real parts of *s* in the table are not exactly zero, but are taken to be computationally zero if their absolute values are less than 10^{-3}

Finally, the data of Table 2 show that as the relative gap-width decreases, so do the values of $\mathscr{R}_c$ As the gap-width decreases toward zero, the upper and lower parts of the annulus become more like horizontal, parallel, rigid plates The lower region is stably stratified since the warmer surface is above the cooler, while the upper region is potentially unstable The equatorial region behaves more like vertical, parallel, rigid plates with one plate warmer than the other Consequently, it is expected that the critical stability parameter should approach that for horizontal, parallel, rigid–rigid plates (the Rayleigh–Bénard problem), being $Ra_c = 1708$ (for critical wave number $a_c = 3\ 117$) [8] Since $Ra_c = Gr_c\ Pr = \mathscr{R}_c^2\ Pr$, the equivalent value in terms of $\mathscr{R}_c$ is

$$\mathscr{R}_{c_{\varepsilon\to 0}} = \frac{41.33}{\sqrt{(Pr)}} \tag{23}$$

The values of $\mathscr{R}_{c_{\varepsilon\to 0}}$ given by equation (23) then provide lower bounds to the results of this paper In Table 2, data are given for $\varepsilon = 0\ 050$ for $Pr \geqslant 0.7$ The data

Table 4. Critical eigenvalues for Prandtl numbers near Pr_t showing the change from steady to time-periodic bifurcation of the basic flow

$\varepsilon = 0\ 100$		$\varepsilon = 0.075$	
Pr	*s*	*Pr*	*s*
0.250	$-1\ 764\times 10^{-6}+i12\ 631$	0 23	$-8\ 740\times 10^{-4}+i8.097$
0 270	$-9\ 797\times 10^{-6}+i12\ 820$	0.25	$-1.343\times 10^{-6}+i8\ 226$
0 290	$-5\ 229\times 10^{-6}+i13\ 107$	0.27	$-4.926\times 10^{-6}+i8.317$
0 300	$1\ 347\times 10^{-6}+i0$	0 28	$-3\ 947\times 10^{-4}+i8.368$
0 305	$2\ 245\times 10^{-5}+i0$	0.29	$5\ 614\times 10^{-4}+i0$
0 310	$3\ 631\times 10^{-5}+i0$	0 30	$9\ 346\times 10^{-6}+i0$

confirm the trend to the predicted lower bound. Consider $Pr = 0.7$ The value of $\mathscr{R}_{c_{\varepsilon \to 0}} = 49.4$, which compares with 50 3 for $\varepsilon = 0\ 050$

4. CONCLUSIONS

Central to this research was the computation of a neutral stability map showing the dependence of the critical stability parameter $\mathscr{R}_c$ on Pr for each ε Each neutral curve was found to be a monotone decreasing function of the Prandtl number A characteristic of each neutral curve was found to be the presence of a transitional Prandtl number dividing the curve into distinct structures. Values of Pr_t were found to be 0 30 for $\varepsilon = 0.100$ and 0.28 for $\varepsilon = 0\ 075$ For $Pr > Pr_t$, the structure is linear on a log–log plot having a slope of $-1/2$ That is

$$\mathscr{R}_c = \frac{C(\varepsilon)}{\sqrt{(Pr)}}$$

where $C(\varepsilon)$ is a proportionality coefficient dependent on the relative gap-width, ε When $Pr < Pr_t$, the structure is non-linear approaching an upper bound at $Pr = 0$. It was also found that as the gap-width decreased, the values of $\mathscr{R}_c$ approached those for the Rayleigh–Bénard stability problem.

The results presented in this work confirm the hypothesis stated in the Introduction that the observed changes in the pattern of the basic motion for certain flow parameter values are due to instability of the basic motion. The results indicate that for Prandtl numbers larger than Pr_t, the unstable flows evolve to a steady pattern while for smaller Prandtl numbers the bifurcated flows are time periodic.

Finally, the results found here conform to the experimental observations of basic flow transition as shown in Fig 1 for air ($Pr \approx 0\ 7$) Although observations were made for larger ε than considered here, an extrapolation of the data to narrower gap-widths shows a reasonable trend to the data found in this research The visualization results suggest that the bifurcated flow field (the 'Falling Vortices' flow pattern) is unsteady and three-dimensional (at least for $\varepsilon > 0\ 15$), while the results found here for $\varepsilon < 0.1$ predict a steady bifurcated flow which is by definition two-dimensional The implication is that the critical values presented here are true upper bounds to the critical values for the bifurcation

Acknowledgements—This material is based upon work supported by the National Science Foundation under Grant No CBT-8612427 In addition, this work was partially supported by the National Center for Supercomputing Applications and utilized the CRAY 2 system at the National Center for Supercomputing Applications at the University of Illinois at Urbana–Champaign Partial support was also provided by the Department of Mechanical Engineering and the College of Engineering and Technology of the University of Nebraska–Lincoln This support is gratefully acknowledged

REFERENCES

1 M T Farmer, R W Douglass and S A Trogdon, The stability of natural convection in narrow-gap spherical annuli to axisymmetric disturbances, *Int J Heat Mass Transfer* **29**, 1575–1584 (1986)
2 E H Bishop, R S Kolflat, L R Mack and J A Scanlan, Convective heat transfer between concentric spheres, *Proc 1964 Heat Transfer and Fluid Mech Inst*, pp. 69–80. Stanford University Press, Stanford, California (1964)
3 S H Yin, Natural convective flow between isothermal concentric spheres, Ph.D thesis, Montana State University, Bozeman, Montana (1972).
4. S H. Yin, R. E Powe, J A Scanlan and E H Bishop, Natural convection flow patterns in spherical annuli, *Int J. Heat Mass Transfer* **16**, 1785–1795 (1973)
5 D R Gardner, Linear stability and bifurcation of natural convection flows in narrow-gap, concentric spherical annulus enclosures, Ph D thesis, University of Nebraska–Lincoln, Lincoln, Nebraska (1988)
6 J L. Wright and R W Douglass, Natural convection in narrow-gap spherical annuli, *Int J Heat Mass Transfer* **29**, 725–739 (1986)
7 D. R Gardner, S A Trogdon and R. W Douglass, A modified tau spectral method that eliminates spurious eigenvalues, *J. Comp Phys* **80**, 137–167 (1989).
8 P G Drazin and W H Reid, *Hydrodynamic Stability*, p 51. Cambridge University Press, New York (1981)
9 L R Mack and H C. Hardee, Natural convection between concentric spheres at low Rayleigh numbers, *Int. J Heat Mass Transfer* **11**, 387–396 (1968)
10 S N Singh and J. Chen, Numerical solution for free convection between concentric spheres at moderate Grashof numbers, *Numer. Heat Transfer* **3**, 441–459 (1980)
11 R J. Brown, Natural convection heat transfer between concentric spheres, Ph D thesis, University of Texas–Austin, Austin, Texas (1967)
12. K N Astill, H. Leong and R. Martorana, A numerical solution for natural convection in concentric spherical annuli In *Natural Convection in Enclosures* (Edited by K E Torrence and I Catton), HTD-Vol 8, pp. 105–113 The American Society of Mechanical Engineers (1980)
13. J-P Caltagirone, M Combarnous and A Mojtabi, Natural convection between two concentric spheres transition toward a multicellular flow, *Numer Heat Transfer* **3**, 107–114 (1980).
14 D B Ingham, Heat transfer by natural convection between spheres and cylinders, *Numer Heat Transfer* **4**, 53–67 (1981)

EFFETS DU NOMBRE DE PRANDTL SUR LA STABILITE DE LA CONVECTION NATURELLE ENTRE DES SPHERES

Résumé—On présente une analyse de l'effet du nombre de Prandtl sur la stabilite linéaire des perturbations axisymetriques ($m = 0$) pour une convection naturelle permanente entre deux parois concentriques sphériques, lorsque l'espace est étroit Les équations de perturbation sont resolues en utilisant une série spectrale tronquée On examine la convergence de la serie Les nombres de Prandtl sont compris entre 0 et 100, tandis que l'espacement relatif est égal à 0,100, 0,075 et 0,050 Les résultats confirment l'hypothèse que les changements observés expérimentalement dans le mouvement de base, pour certains paramètres d'écoulement, sont dûs à l'instabilite et ils indiquent que pour un nombre de Prandtl quelconque plus grand qu'une valeur de transition, les écoulements instables evoluent vers une configuration stable, tandis que pour de plus petits nombres de Prandtl les ecoulements bifurqués sont periodiques dans le temps

EINFLUSS DER PRANDTL-ZAHL AUF DIE STABILITÄT DER NATURLICHEN KONVEKTION ZWISCHEN KUGELSCHALEN

Zusammenfassung—Eine Analyse des Einflusses der Prandtl-Zahl auf die lineare Stabilitat von achsensymmetrischen ($m = 0$) Storungen bei stationarer naturlicher Konvektion in konzentrischen Kugelschalen mit kleinen Spaltweiten wird vorgestellt Die Storungsgleichungen werden mittels einer abgebrochenen Spektralreihe gelost Die Konvergenz dieser Reihe wird uberpruft Der Bereich der Prandtl-Zahlen erstreckt sich von 0 bis 100, der Bereich der relativen Spaltweite betragt 0,1, 0 075 und 0,050 Die Ergebnisse bestatigen die Annahme, daß die im Experiment beobachteten Änderungen der grundlegenden Bewegung bei gewissen Stromungsparametern auf eine Instabilität zuruckzufuhren sind Die Ergebnisse zeigen, daß fur jede Prandtl-Zahl oberhalb eines bestimmten Übergangswertes die instabilen Stromungen in einen stationaren Zustand ubergehen, während für kleinere Prandtl-Zahlen periodisch gegabelte Stromungen auftreten

ВЛИЯНИЕ ЧИСЛА ПРАНДТЛЯ НА УСТОЙЧИВОСТЬ ЕСТЕСТВЕННОЙ КОНВЕКЦИИ МЕЖДУ СФЕРИЧЕСКИМИ ОБОЛОЧКАМИ

Аннотация—Анализируется влияние числа Прандтля на линейную устойчивость осесимметричных ($m = 0$) возмущений стационарной естественной конвекции между двумя концентрическими сферическими оболочками, расположенными с узким зазором. Уравнения возмущений решаются для усеченного спектрального ряда Рассматривается сходимость рядов. Значения числа Прандтля изменяются от 0 до 100, а относительная ширина зазора составляет 0,100; 0,075 или 0,050. Полученные результаты подтверждают гипотезу о том, что экспериментально наблюдаемые изменения основного течения при определенных параметрах течения обусловлены его нестационарностью и означают, что при любом значении числа Прандтля выше переходного нестационарное течение выходит на стационарный режим, в то время как при низких значениях числа Прандтля бифуркационные течения являются периодическими во времени